AN ABSTRACT OF THE THESIS OF

Bryan J. Norton for the degree of Master of Science in Physics presented on June 3, 2005.

Title: Generation and Pulse Shaping of Multi-Cycle Terahertz Waves Through Manipulation of Femptosecond Optical Pulses

Abstract approved:

Redacted for privacy

Yun-Shik Lee

We used two temporally separated femtosecond pulses to manipulate the waveforms of multi-cycle THz pulses through optical rectification in periodically-poled lithium niobate (PPLN). The relative phase of the THz pulses was controlled by the relative time delay between the optical pulses. This phase adjustability combined with the frequency tunability of the PPLN sample enables the pulse shaping of multi-cycle narrow-band THz pulses. The THz pulse shaping technique is applicable to coherent control of molecular excitations and of carrier population in semiconductors.

Generation and Pulse Shaping of Multi-Cycle Terahertz Waves Through Manipulation of Femptosecond Optical Pulses

By

Bryan J. Norton

A THESIS

submitted to

Oregon State University

in partial fulfillment of
the requirements for the
degree of

Master of Science

Presented June 3, 2005
Commencement June 2006

Master of Science thesis of Bryan J. Norton presented on June 3, 2005.

APPROVED:

Redacted for privacy

Major Professor, representing Physics

Redacted for privacy

Chair of the Department of Physics

Redacted for privacy

Dean of the Graduate School

I understand that my thesis will become part of the permanent collection of Oregon State University libraries. My signature below authorizes release of my thesis to any reader upon request.

Redacted for privacy

Bryan J. Norton, Author

CONTRIBUTIONS

I would like to express gratitude to Dr. Yun-Shik Lee, Naaman Amer, and Walter Hurlbut for their support, guidance, and assistance in the data collection for this paper.

TABLE OF CONTENTS

Page

LIST OF FIGURES

GENERATION AND PULSE SHAPING OF MULTI-CYCLE TERAHERTZ WAVES THROUGH MANIPULATION OF FEMPTOSECOND OPTICAL PULSES

1. INTRODUCTION

1.1. Overview

There is a little known section of the electromagnetic spectrum just below infrared known as terahertz (THz) that has recently emerged from obscurity. The THz region of the electromagnetic spectrum is loosely defined by the range of frequencies 0.1 to 10 THz (Figure 1). In the last ten years, much progress has been made in the generation and detection of THz radiation. This advancement has opened up the previously unreachable THz range.

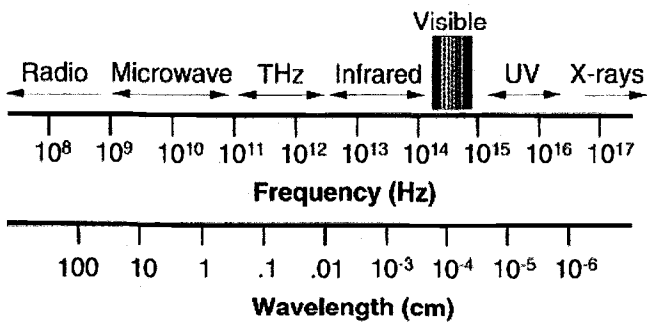

Figure 1. The electromagnetic spectrum depicting the THz region between the microwave and infrared [13].

The two most prevalent methods of generating coherent radiation are the laser and the antenna, both of which miss the THz range. The dipole antenna generates radiation by accelerating electrons up and down an antenna wire. Transistors commonly control this acceleration. Modern transistors switch only as fast as gigahertz, which is three orders of magnitude too slow. Lasers, on the other hand, rely on pumping a medium and stimulating emission in a coherent manner. The energy of a THz wave is too low to stimulate an electronic transition necessary for this method.

Femtosecond lasers, which were first demonstrated in 1985 [1], supply a pulse fast enough to generate THz. This laser, through the use of mode-locking, can generate a pulse of light as short as 100 femtoseconds (fs) long (100×10^{-15} s). This laser's pulse duration and the wavelength of THz radiation are of similar length. The femtosecond laser is the first device to provide switching capabilities fast enough to control THz sources. This short laser pulse has been used to control the aforementioned dipole antenna. This technique uses a photoconductive antenna to generate THz, much as a radio transmitter does.

Radiation generated by an antenna has an inherent disadvantage from that generated by a laser: laser light is collimated. Collimated light is necessary for many modern optical applications and scientific research areas. The ability to efficiently generate collimated THz radiation is of immense value. To achieve this, we must look to other techniques, namely optical rectification. Optical rectification is a byproduct of a non-linear process called second harmonic generation [2]. The second order term in the polarization leads to a DC component in the reradiated light, which gives the effect of an optical rectifier. This will be discussed in detail later.

1.2. Terahertz Radiation in the Background

According to Planck's law of black body radiation, the energy density of electromagnetic radiation from a black body at temperature T is given by the formula:

$$\rho(\lambda,T)d\lambda = \frac{8\pi hc}{\lambda^5 e^{\frac{hc}{\lambda kT}} - 1} d\lambda . \qquad (1)$$

The energy density above has been plotted for a range of temperatures in Figure 2 below.

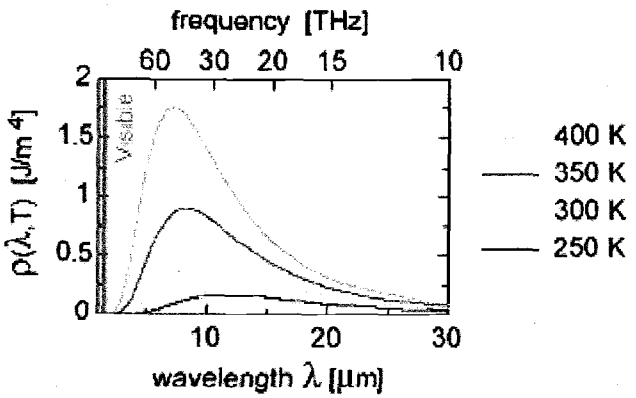

Figure 2. Plot of black body radiation for a range of temperatures.

Wien's displacement law states that there is an inverse relationship between the wavelength of the peak of the emission and its temperature,

$$\lambda_{max} \cdot T = 2.89x10^{-3}\, Km\,. \tag{2}$$

For room temperature, ρ_{max} = 0.4J/m4 is around 10 μm (30 THz). In the upper part of the defined THz range – around 10 THz – one still has a spectral energy density of 0.05J/m^4. This value then decreases rapidly to 1.3x10-9 J/m^4 for 0.1 THz. As a consequence of Planck's radiation law, every object at room temperature radiates at frequencies in the THz range. Hence, THz radiation is a ubiquitous natural phenomenon.

1.3. Terahertz Interaction with Matter

Due to the newness of THz as an area of study, how the THz spectrum interacts with matter is not as well known as that of the rest of the electromagnetic field. Following is a list of examples of how THz interacts with matter.

- THz radiation is, depending on its corresponding photon energy of a few meV, classified as non-ionising radiation. According to the current state of research, THz radiation is thus harmless to cellular structures like the human body. As a result, the potential of THz for biological applications is obvious. Some day, THz tomography could become an interesting compliment to X-ray radiography and other diagnostic techniques.

- Phonons are, by the majority, in the THz range. As a consequence, THz absorption spectra can be used to classify different materials.

- The vibrational modes of water and water vapor also lie in the THz range. This means that water is not transparent for THz radiation. Furthermore, the atmospheric moisture absorbs much of the radiation, which is a problem for many THz experiments.

- Dielectrics (e.g. paper, plastics) are highly transparent for THz. This property is responsible for THz having interesting applications in imaging and remote sensing.

- Metals reflect almost any radiation and hence have huge absorption constants in this spectral range.

1.4. Applications

With THz, it is possible to probe a vast variety of systems such as: intersubband transitions in semiconductors [3], vibrational levels in molecules [4], and phonon resonances in crystals [5]. Other practical applications for imaging with THz beams are also being developed [6], including biomedical usage, quality control, and security. THz waves offer unique measurement capabilities. Optical detectors only measure the intensity of light, and thus lose all phase information. When measuring THz beams, we can measure both the amplitude and phase of the THz electric field directly.

One of the major applications of THz spectroscopy systems is in material characterization, particularly of lightweight molecules and semiconductors. Terahertz spectroscopy has been used to determine the carrier concentration and mobility of doped semiconductors such as gallium arsenide (GaAs) and silicon wafers [7]. The Drude model may then be used to link the frequency-dependent dielectric response to the material free-carrier dynamic properties, including the plasma angular frequency and the damping rate [8]. A focus is on the measurement of experiments with optical-pump/THz-probe systems, which can reveal additional information about materials [9]. In these experiments, the material is excited using an ultra fast optical pulse, and a THz pulse is used to probe the dynamic far-infrared properties of the excited material.

1.5. THz Time-Domain Spectroscopy

Terahertz time-domain spectroscopy (THz-TDS) uses short pulses of broadband THz radiation, which are typically generated using ultra fast laser pulses [10]. This technique grew from work in the 1980s at AT&T Bell Labs and the IBM T. J. Watson Research Center. Although the spectral resolution of THz-TDS is much coarser than narrowband techniques, it has a number of advantages that have given rise to some important recent applications. The transmitted THz electric field is measured coherently, which provides both high sensitivity and time-resolved phase information. It is also amenable to implementation within an imaging system to yield rich spectroscopic images. Typical THz-TDS systems have a frequency bandwidth between 0.3 and 3 THz and a spectral resolution of 50 GHz.

2. THEORY OF THZ GENERATION

2.1. THz Generation by Optical Rectification

A non-centro symmetric, nonlinear crystal, in the presence of an intense optical beam, exhibits a well-known nonlinear optical effect called frequency doubling. This process can be understood by examining the second order nonlinear polarization term where the electric field is squared, as shown below:

$$P = \chi_2 E^2 . \tag{3}$$

We take the electric field to be a sinusoidal plane wave at frequency ωt:

$$E = E_0 Cos(\omega t), \tag{4}$$

which can be expanded to

$$E^2 = [E_o Cos(\omega t)]^2 = E_0^2 Cos^2(\omega t) = \frac{1}{2} E_0^2 + \frac{1}{2} E_0^2 Cos(2\omega t). \tag{5}$$

When we square the plane wave, and expand it with a trigonometric identity into its frequency components, we get a frequency doubled part and a DC part. The DC part is what we are interested in because its shape is proportional to the wave's amplitude. If we make a wave packet on the femtosecond scale, we will get an optically rectified wave out also on the femtosecond scale. Figure 3 below depicts this process; a femtosecond wave packet is incident from the left on a zinc telluride (ZnTe) nonlinear crystal. A femtosecond pulse is produced.

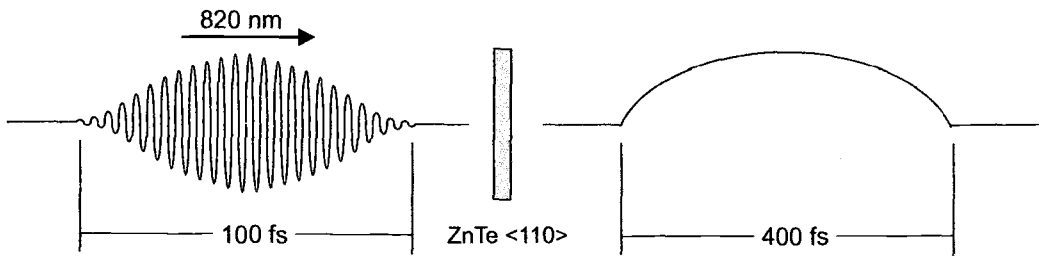

Figure 3. Optical rectification of a femtosecond pulse in ZnTe.

THz generation by optical rectification is possible by use of a femtosecond laser beam. The following derivation can be found in Reference 11. For our model, we assume a Gaussian pulse traveling in the z-direction. The mathematics is easer to do in the frequency domain. Below we have our pulse in the form of a Fourier integral:

$$E(t,z) = \int_{-\infty}^{\infty} E_0 e^{-(\omega-\omega_o)^2\tau_p^2} e^{i(\omega t - k(\omega)z)} d\omega . \tag{6}$$

In general, non-linear crystals are dispersive so k depends on ω. To a good approximation, we can expand k(ω) around ω_o in $(\omega-\omega_o)$ including only the first order term. Higher order terms are neglectable because the integrand is killed off by the Gaussian when ω is a small distance from ω_o. Let

$$k(\omega) = k(\omega_o) + \left.\frac{dk}{d\omega}\right|_{\omega_o} (\omega - \omega_o) \tag{7}$$

where

$$\frac{dk}{d\omega} = \frac{1}{v_g} = \frac{n_g(\lambda)}{c} = \frac{n(\lambda) - \frac{\partial n}{\partial \lambda}\lambda}{c} \tag{8}$$

with v_g, the group velocity of the pulse, and $n(\lambda)$, the index of refraction for a given wavelength λ. Putting this approximation into the integrand and evaluating yields, we get:

$$E(t,z) = \widetilde{E} \cdot e^{\frac{(t-\frac{z}{v_g})^2}{4\tau_p^2}} e^{i(\omega_o t - k(\omega_o)z)} \tag{9}$$

where

$$\tau_p = \frac{D_{fwhm}}{\sqrt{8\ln 2}} \tag{10}$$

with D_{fwhm}, the full width half max of the laser pulse. Using two of Maxwell's equations,

$$\nabla \times E(r,t) + \mu_o \frac{\partial H(r,t)}{\partial t} = 0 \tag{11}$$

and

$$\nabla \times H(r,t) = j(r,t) + \frac{\partial D(r,t)}{\partial t}. \tag{12}$$

Assuming the medium is nonconductive $\sigma = 0$, and that there is no free charge (*div*E=0), we find a relation between the electric field and the displacement vector D:

$$\Delta E(r,t) = \mu_o \frac{\partial^2 D(r,t)}{\partial t}. \tag{13}$$

When dealing with pulses, it is commonly easier to evaluate in the frequency domain. So, we will write the electric and displacement fields in terms of a Fourier integral:

$$\Delta \int_{-\infty}^{\infty} E(r,w) \cdot e^{i\omega t} d\omega = \mu_o \frac{\partial^2}{\partial t^2} \int_{-\infty}^{\infty} D(r,\omega) \cdot e^{i\omega t} d\omega. \tag{14}$$

The second time derivative can be moved inside the integral and, once evaluated, we can make the following statement:

$$\Delta E(r,\omega) = -\omega^2 \mu_o D(r,w). \tag{15}$$

Remembering the definition for the displacement field,

$$D(r,\omega) = \varepsilon_o E(r,\omega) + P_L(r,w) + P_{NL}(r,\omega) = \varepsilon_o(1+\chi_1(\omega))E(r,\omega) + P_{NL}(r,\omega) \quad (15)$$

Combining the two above equations yields the wave equation below:

$$\Delta E(r,\omega) + \frac{\varepsilon(\omega)\omega^2}{c^2} E(r,\omega) = -\mu_o \omega^2 P_{NL}(r,\omega) \quad (16)$$

where the P_{NL} term is the source of the nonlinear response.

The above equation is the key to understanding how this process can generate THz radiation. Below is just the DC component of the polarization (the optically rectified pulse):

$$P_{NL}(r,t) = \frac{1}{2}\varepsilon_o \chi_2 \tilde{E}_o^2 \cdot e^{\frac{\left(t-\frac{z}{v_g}\right)^2}{2\tau_p^2}} = p_o \cdot e^{\frac{\left(t-\frac{z}{v_g}\right)^2}{2\tau_p^2}} . \quad (17)$$

Assuming no dispersion in χ_2, the Fourier components of the pulse are below:

$$P_{NL}(r,\omega) = \frac{P_o}{\sqrt{2\pi}} \tau_p e^{-\frac{\omega^2 \tau_p^2}{2}} e^{-i\omega\frac{z}{v_g}} . \quad (18)$$

Putting it all together the source term from the wave equation is

$$-\mu_o \omega^2 P_{NL}(r,\omega) = -\mu_o \omega^2 \frac{P_o}{\sqrt{2\pi}} \tau_p e^{-\frac{\omega^2 \tau_p^2}{2}} e^{-i\omega\frac{z}{v_g}} = a_o \omega^2 \tau_p e^{-\frac{\omega^2 \tau_p^2}{2}} e^{-i\omega\frac{z}{v_g}} . \quad (19)$$

The amplitude of the source is given below:

$$a(\omega) = a_o \omega^2 \tau_p e^{-\frac{\omega^2 \tau_p^2}{2}} . \quad (20)$$

In the next figure the amplitude a(ω) is shown for different pulse lengths.

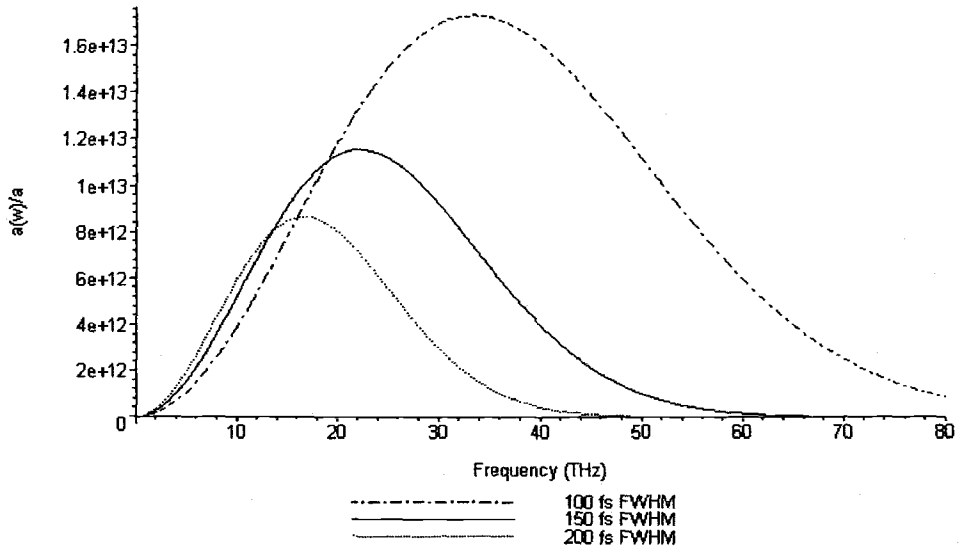

Figure 4. Amplitude of the source term for THz radiation for a set of pulse durations.

2.2. Periodically Poled Lithium Niobate

THz radiation generation through optical rectification in ZnTe has proven to be an enormously valuable technique as evidenced by the large number of published papers and advancements in the field. However, it is not without its shortcomings, the most noteworthy of which is that optical rectification supplies us with only one cycle of THz radiation. This fact has been widely exploited in broadband THz time domain spectroscopy. THz, like any other spectral range, will need narrow band sources as well as broad. In 2002, a new technique for generating THz through optical rectification using periodically poled lithium niobate (PPLN) was proposed [12]. Lithium niobate has a dramatic group velocity mismatch between THz and optical radiation. This allows generation of THz pluses, whose shape is dependent on the domain structure of an engineered lithium niobate crystal. The PPLN sample is grown with alternating susceptibility in a periodic fashion. The second polarization

term is dependent on the square of the electric field and the susceptibility tensor. So, the direction of the induced polarization is dependent on the direction of the tensor and not the incident electric field. This is a big part of what allows generation of a multi-cycle wave from a pulse. As the optical pulse travels through the PPLN crystal, it encounters domains of alternating susceptibility directions: first up, then down, then up, and so on. Since the polarization is dependent on the susceptibility and not the electric field, the THz radiation reflects the periodic structure of the crystal. The optical pulse travels faster than the THz, thus forming the periodic polarization before the THz pulse can exit the crystal entirely. This means that the first cycle of the THz pulse to be formed is the last to exit the crystal. The optical pulse will lead the THz by

$$t = \frac{d_w(n_{THz} - n_{opt})}{c}. \tag{21}$$

If we engineer our domain structure to be comparable to d_w, each domain will form a half-cycle of our THz wave. The wavelength of the THz is proportional to the domain spacing, which allows us to control the frequency of our generated THz accordingly.

To calculate the THz field, we assume that our optical pulse from the mode-locking laser is Gaussian, as earlier derived. If this optical pulse is traveling in the z direction, the THz field per unit length can be expressed as:

$$\varepsilon_L(z,t) = \varepsilon_0\left[\frac{2(z-v_0t)^2}{V_0^2\tau^2} - 1\right]\exp\left[\frac{(z-v_0t)^2}{v_0^2\tau^2}\right] \tag{22}$$

where τ is the optical pulse duration and v_o the optical group velocity.

The THz field as it exits the crystal can be expressed as:

$$E_{THz}(t) = \int_0^L \pm\varepsilon_L\left[z'-v_0\left(t-\frac{L-z'}{v_t}\right)\right]dz' = \sum_{i=1}^{N}(-1)^{i-1}\int_{l_i-1}^{l_i}\varepsilon_L\left[z'-v_o\left(t-\frac{L-z'}{v_t}\right)\right] \tag{23}$$

where L is the length of the crystal, l_i is the position of the ith domain interface, N is the number of domains, and v_t is the THz group velocity. The sign of the THz field is dependent on the direction of the susceptibility tensor. In the second equation, we assume that each domain is flipped.

If we neglect the dispersion of the optical and THz pulses, we can evaluate the integration for each domain:

$$\int_{l_{i-1}}^{l_i} \varepsilon_L dz' = \frac{\varepsilon_0}{1-\frac{v_0}{v_t}} \left[-\xi e^{-\frac{\xi^2}{v_0^2 \tau^2}} \right]_{\xi(i-1)}^{\xi}, \tag{24}$$

where

$$\xi_i = \left(1-\frac{v_0}{v_t}\right) l_i + \frac{v_0}{v_t} L - v_0 t . \tag{25}$$

Thus, the analytic solution is below:

$$E_{THz}(t) = \sum_{i=1}^{N} (-1)^{i-1} \left[E_i(t) - E_{i-1}(t) \right] \tag{26}$$

$$E_i(t) = \frac{\varepsilon_0 \xi_i}{\frac{v_0}{v_t} - 1} e^{-\frac{\xi_i^2}{v_0^2 \tau^2}} \tag{27}$$

The power of this technique becomes evident through this derivation. We cannot only make narrow band periodic pulses, but also arbitrary wave shapes by changing the spacing between domains. Below are three examples of what can be done by changing the domain spacing.

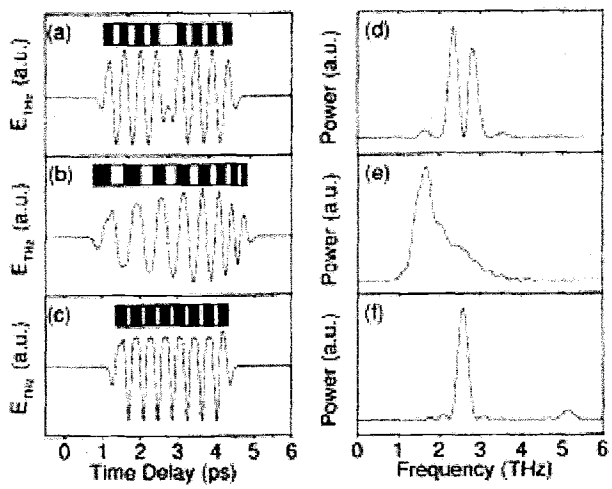

Figure 5. Demonstration of domain structure synthesized waveforms [11].

For all of the above calculations, the optical pulse duration was set to 200 fs. In Figure 5, diagram (a) shows a zero area double pulse. This waveform consists of two pulses the have a Pi phase shift in the center. This was created by simply increasing the center domain spacing to 40 μm compared to the rest of the domains, which are 20 μm. Diagram (b) in Figure 5 shows a chirped THz pulse. The crystal consists of 15 domains ranging from 10-40 μm. In Figure 5, diagram (c) is a sample with alternating domain length. It can be seen, from the time domain representation of the pulse, that the pulse matches the domain structure.

2.3. Tunable THz

Narrowband sources are extremely valuable in spectroscopy. Equally important would be the ability to have a continuously tunable source. Using the domain structure as described above, we can make crystals to generate arbitrary THz frequencies. This requires a different crystal for each frequency. While this would provide the ability to generate a specific frequency, continuous tunability is still not achieved. If we engineer a sample with the geometry below, tunability can be

achieved [13]. By focusing the laser on different parts of the sample, the pulse travels through different domain spacing and thus generates different THz frequencies. This is demonstrated in Figure 6 below. The dots represent experimental data verifying the frequency spectrum that can be generated with a PPLN sample.

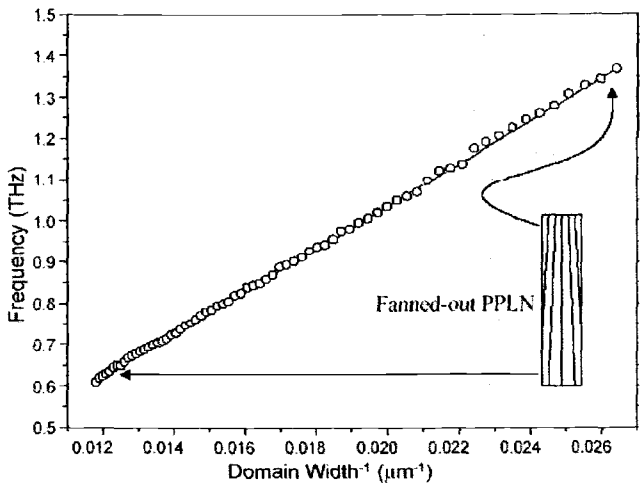

Figure 6. Experimental demonstration of PPLN fanned-out sample [11].

3. THEORY OF THZ WAVE DETECTION

3.1. Electro-Optic Effect

In our experimental setup, we use electro-optic sampling to detect the THz wave. This technique allows us to measure both the amplitude and the phase of the THz electric field [13]. Herein lies the power of electro-optic sampling. Without this additional information, THz time domain spectroscopy would not be possible.

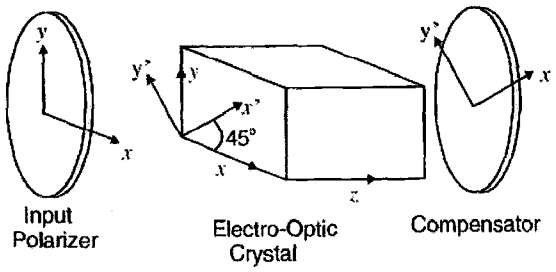

Figure 7. Electro-optic crystal.

The electro-optic effect can be understood in the following way. Derivation can be found in Reference 14. In Figure 7, the probe beam is propagating in the z direction; x and y label the crystal axes of the electro-optic crystal. If an electric field is applied to the crystal, the induced birefringence axes x' and y' are at an angle of 45° with respect to x and y. If the input beam is polarized along the x axes, the electric field of the output light is given below:

$$\begin{pmatrix} E_x \\ E_y \end{pmatrix} = \begin{pmatrix} \cos\left(\frac{\pi}{4}\right) & -\sin\left(\frac{\pi}{4}\right) \\ \sin\left(\frac{\pi}{4}\right) & \cos\left(\frac{\pi}{4}\right) \end{pmatrix} \cdot \begin{pmatrix} e^{i\delta} & 0 \\ 0 & 1 \end{pmatrix} \cdot \begin{pmatrix} \cos\left(\frac{\pi}{4}\right) & -\sin\left(\frac{\pi}{4}\right) \\ \sin\left(\frac{\pi}{4}\right) & \cos\left(\frac{\pi}{4}\right) \end{pmatrix} \tag{28}$$

where $\delta=\Gamma_o+\Gamma$ is the phase difference between the x' and y' polarizations. Γ_o is generated by the intrinsic birefringence of the crystal and compensator, and Γ is the birefringence induced by the electric field. From the equation above, we can find the intensities of the two polarizations shown below:

$$|E_x| = I_o \cos^2 \frac{\Gamma_0 + \Gamma}{2} = I_x \tag{29}$$

and

$$|E_y| = I_o \sin^2 \frac{\Gamma_0 + \Gamma}{2} = I_y \tag{30}$$

with I_o being the input intensity.

The phase term Γ_o must be $\pi/2$ for balanced detection, i.e. $I_x \cong I_y$ for E=0. ZnTe has no intrinsic birefringence. In such a case, a quarter-wave plate is used to provide the phase shift. In most practical applications, $|\Gamma| << 1$. Thus, we can make simplifying approximations to obtain

$$I_x = I_o \frac{1-\Gamma}{2} \tag{31}$$

and

$$I_y = I_o \frac{1+\Gamma}{2}. \tag{32}$$

Experimentally, a Wollaston prism is used to split the beam into x and y polarization as shown above. In the balanced detection scheme, the difference between the intensities is measured giving

$$I_s = I_y - I_x = I_o \Gamma. \tag{33}$$

In this equation, Γ is proportional to the electric field that induces the birefringence. For a <110> oriented ZnTe crystal, the below relation applies:

$$\Gamma = \frac{\pi d n^3 \gamma_{41}}{\lambda} E \tag{34}$$

where d is the crystal thickness, n is the refractive index of the crystal at the probe beam's wavelength, λ is the probe wavelength , γ_{41} is the electro-optic coefficient, and E is the electric field of the THz pulse. So the electric field can be expressed as follows:

$$E = I_s \frac{\lambda}{I_o \pi d n^3 \gamma_{41}}. \tag{35}$$

3.2. Wollaston Prism

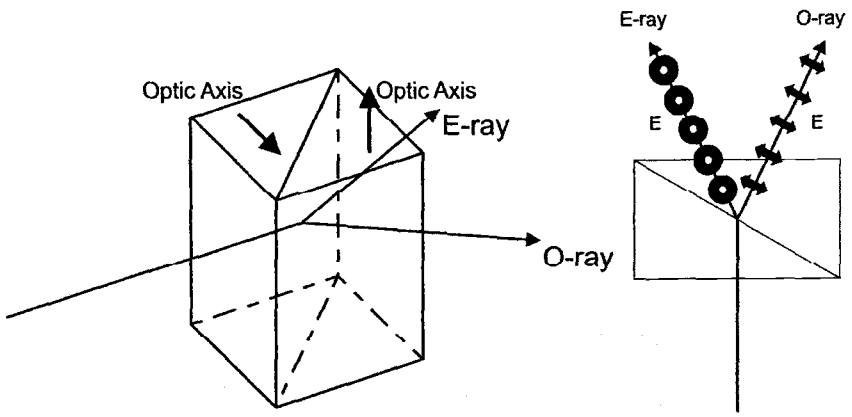

Figure 8. Wallaston Prism.

The Wollaston prism has the ability to split a beam into its two polarizations, as depicted in Figure 8 above. It consists of two right triangle prisms with perpendicular optic axes. At the interface, the extraordinary-ray in the first prism becomes an ordinary-ray in the second and is bent toward the normal. The ordinary-ray becomes an extraordinary-ray and is bent away from the normal. The beams diverge from the prism, giving two perpendicular polarized rays. The angle of divergence of these two rays is determined by the wedge angle of the prisms. [15]

4. FEMTOSECOND LASER THEORY

4.1. Description of Mode-Locking Laser

To generate THz through optical rectification as described above, an intense femtosecond pulse is required. Lasers capable of generating pulses shorter than 100 fs were demonstrated in 1981. By 1987, femtosecond pulses as short as 6 fs were observed at Bell Laboratories [14]. In the last 20 years, much progress has been made in the field of ultra fast optics because of its interesting applications. These ultra short pulses can be used to time resolve the steps of chemical reactions. Also, nonlinear

optics is critically dependent on short, high intensity pulses, of which femtosecond pulses are the shortest with very high peak intensities (up to petawatts).

For our experiment, we used a solid-state femtosecond laser. Our solid-state femtosecond laser consists of a crystal lasing medium (Titanium-doped Sapphire) in a mode-locking optical cavity. A laser is mode-locked when many longitudinal modes inside the laser cavity are held in phase. Consequently, an intense pulse is formed through constructive interference of the modes producing the femtosecond pulse. The extremely short duration of the femtosecond pulse produces enormous peak power.

The core of any laser is its lasing medium. In our case, it is a Titanium Sapphire (Ti:Sapph) crystal. Titanium Sapphire has an energy level configuration typical of any four-level solid-state laser. However, the unique properties of this material are: (1) its broad absorption band that can be populated by a fixed-frequency laser, and (2) the wide bandwidth over which the lasing can occur. This is important because our Ti:Sapph is going to be lasing short pulses – the shorter the pulse the wider the bandwidth. Titanium Sapphire is attractive for a femtosecond laser because it has enough bandwidth to lase 3 fs pulses.

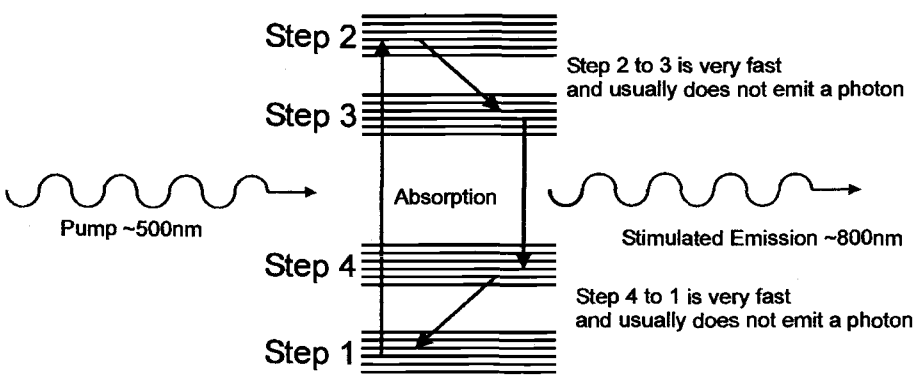

Figure 9. Energy level diagram for Titanium Sapphire.

Figure 9 above shows the energy levels of Titanium Sapphire. The absorption band peaks at around 500 nm, and the emission spectrum peaks around 800 nm. In Figure 9 above, we see four steps, each one an energy band. The fact that they are energy bands is of crucial importance. If they were single states, the pump energy would need to be exactly the difference between them. This would make pumping very difficult and inefficient. Also, if the transition between steps 3 and 4 is not a band transition, mode-locking would not be possible because it would only support one mode (many modes are required for mode locking). The transitions from 2 to 3 and 4 to 1 have a small energy gap, so it takes little time for the state to decay in a non-radiative manner. The non-radiative transitions 2 to 3 and 4 to 1 use up energy from the pump photon making the emitted photon of smaller energy than the absorbed. The large gap in energy between the absorption and emission minimizes losses due to re-absorption of lasing light.

If we place Ti:Sapph in an optical cavity (two mirrors, one highly reflective and one partially), we have the perfect optical oscillator for supporting many longitudinal modes.

The total field created by these many modes can be expressed as the following:

$$E(t) = \sum_{n=1}^{N} E_n e^{(i\omega_n t + \phi_n)} \tag{36}$$

where E_n, ω_n, and Φ_n are the amplitude, frequency, and phase of the n^{th} mode with N the total number of modes. In general, there is no correlation in the phase of the modes as they are said to be incoherent. So, for a large number of modes, the total intensity is just the sum of the individual intensities:

$$I = \sum_{n=0}^{N} E_n^2 . \tag{37}$$

If, however, we fix the phase between the modes at one point, where all the relative phases are zero, we get constructive interference. At this point in space, where all the modes are locked in phase, we get a large electric field – the more modes, the larger the field. In terms of the expression for the electric field above, we can factor the phase term out of the sum:

$$E(t) = E_0 e^{-i\phi} \sum_{n=0}^{n-1} e^{i\omega t} . \tag{38}$$

This sum can be closed with a simple geometric series with the below result:

$$I(t) = E_0^2 \left(\frac{\sin^2\left(\frac{N\pi ct}{2L}\right)}{\sin^2\left(\frac{\pi ct}{2L}\right)} \right) \tag{39}$$

where L is the length of the cavity. Equation 39, the intensity profile of the mode-locking laser, is plotted below in Figure 10.

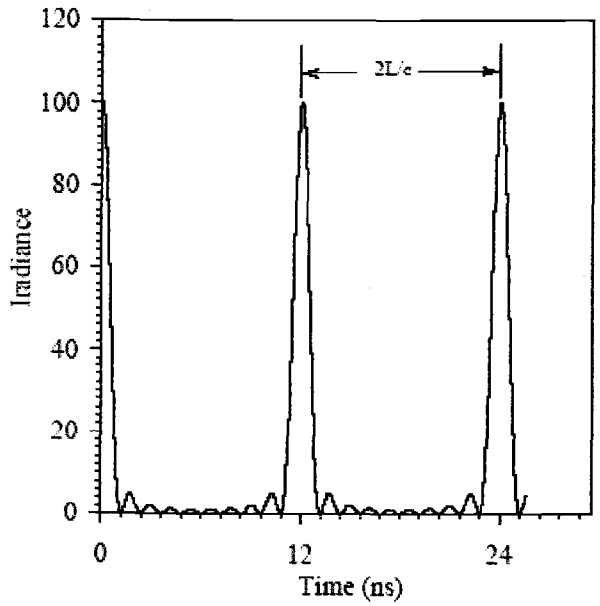

Figure 10. Sink function laser pulses.

The output of the mode-locked cavity is a series of sink functions with period T given by:

$$T = \frac{2L}{c}. \tag{40}$$

4.2. Active Mode-Locking

Now that we understand what mode locking is, and that it would be a great asset, we must have a scheme for locking all the modes in phase. Assume a pulse of light is traveling through a laser cavity [16]. Let E = E_0(z,t)j. We may write,

$$E_0(z,t) = \frac{1}{\sqrt{2\pi}} \int_{-\infty}^{\infty} E_0(\omega) e^{i(kz-\omega t)} d\omega. \tag{41}$$

E_0(z,t) and E_0(w) are Fourier transforms of each other. E_0(w) is the envelope of the pulse in frequency domain, and E_0(t,z) is the envelope of the pulse in time domain. Assume that the laser cavity has length L. It contains a gain medium of length L_g, $L_g \leq L$. The gain in the medium is frequency dependent, so the gain coefficient may be written as:

$$\beta = \frac{\alpha_g L_g}{1 + \left(\frac{\omega - \omega_0}{\omega_0} \right)^2} \tag{42}$$

where ω_0 is the center frequency of the gain medium, ω_g is the width of the gain medium, and $\alpha_g L_g$ is the total gain over the length of the gain medium at the center frequency.

After one trip through the gain medium:

$$E_0(\omega) \rightarrow E_0(\omega) e^{\left(\frac{\alpha_g L_g}{\left(1+\frac{\omega-\omega_0}{\omega_g}\right)^2} \right)}. \tag{43}$$

All laser cavities have losses, so we must include this loss. We model these losses by introducing a loss coefficient α_l in a medium of length L_l, $L_l \leq L$. The total loss over one trip through the loss medium is $a_l L_l$.

So, after one trip through the gain medium:

$$E_0(\omega) \rightarrow E_0(\omega) e^{-\alpha_l L_l}. \tag{44}$$

We now introduce a time dependent loss to cut out modes that are not in phase with the pulse we are locking. This modulated loss is best described in the time domain, i.e. by the way it effects the wave amplitude $E_0(t)$. We model this loss with a medium of length L_m, $L_m << L$. This medium has a loss coefficient $\alpha_m L_m(1-\cos(\omega_m t))$, where ω_m is the modulation frequency.

So, after one trip through the time dependent loss medium:

$$E_0(t) \rightarrow E_0(t) e^{-\alpha_m L_m (1-\cos(\omega_m t))}. \tag{45}$$

We must describe the combined action of gain and loss either in the frequency or in the time domain. If we choose the time domain, take the appropriate Fourier transforms, and keep only first order terms in net gain and loss, then, after one round trip through the cavity, we have:

$$E_0(t+T_R) = \left[1 + 2\alpha_g L_g \left(1 + \frac{1}{\omega_g^2} \frac{d^2}{dt^2}\right) - 2\alpha_l L_l - 2\alpha_m L_m (1-\cos(\omega_m t)) \right] E_0(t) \tag{46}$$

where T_R is the round-trip time of the pulse.

The period of the modulation is $2\pi/\omega_m$. If we want a steady state solution, then we need:

$$\frac{2\pi}{\omega_m} = T_R \text{ and } E_0(t + \frac{2\pi}{\omega_m}) = E_0(t). \qquad (47, 48)$$

Now assume:

$$\frac{2\pi}{\omega_m} = T_R + \delta T_R . \qquad (49)$$

This is to say our time dependent attenuation is slightly off from the round trip time. Then, to first order in δT_R, we may write:

$$E_0(t) = E_0(t)\big|_{\delta T_R = 0} + \delta T_R \frac{dE_0(t)}{dt}. \qquad (50)$$

Including this into equation n, yields:

$$\left[2\alpha_g L_g\left(1 + \frac{1}{\omega_g^2}\frac{d^2}{dt^2}\right) - 2\alpha_l L_l - 2\alpha_m L_m(1 - \cos(\omega_m t)) + \delta T_R \frac{d}{dt}\right] E_0(t) = 0. \qquad (51)$$

This is the equation for active mode locking. It has periodic solutions with period $2\pi/w_m$. Since $2\pi/w_m$ differs slightly from the round trip time T_R of the pulse, the pulse must be pushed into synchronization by reshaping. If $2\pi/w_m < T_R$, then the pulse is advanced by "shaving off" the trailing edge and amplifying the leading edge. If $2p/w_m > T_R$, then the pulse is retarded by "shaving off" the leading edge and amplifying the trailing edge. The pulse becomes narrower.

If we have well-separated pulses that traverse the modulator near the time instant of minimum loss, then we can expand $\cos(w_m t)$ in the above equation, keeping only terms to second order, to obtain the equation for strong mode locking:

$$\left[2\alpha_g L_g\left(1+\frac{1}{\omega_g^2}\frac{d^2}{dt^2}\right)-2\alpha_l L_l-2\alpha_m L_m(\omega_m t)^2+\delta T_R\frac{d}{dt}\right]E_0(t)=0. \quad (52)$$

For the case $\delta T_R = 0$, when the modulation frequency is adjusted so that $2p/w_m = T_R$, this equation becomes equivalent to the one-dimensional Schroedinger equation for a particle in a harmonic-oscillator potential.

The Schroedinger equation

$$\left[\frac{d^2}{dx^2}-\frac{m^2\omega^2}{\hbar^2}x^2+\frac{2mE}{\hbar^2}\right]\psi(x)=0 \quad (53)$$

has solutions

$$\psi_n(x')=H_n(x')e^{-x'^2/2} \quad (54)$$

with $x' = (mw/h)^{1/2}x$, and $E_n = (n + \frac{1}{2})hw$. We may write $x' = w_p x$, and $2mE_n/h^2 = (2n + 1)w_p^2$, with $w_p = (mw/h)^{1/2}$.

For the case $\delta T_R = 0$, the equation for strong mode locking may be written as

$$\left[\frac{d^2}{dt^2}-\frac{\alpha_m L_m \omega_g^2 \omega_m^2}{2\alpha_g L_g}t^2+\omega_g^2\left(1-\frac{\alpha_l L_l}{\alpha_g L_g}\right)\right]E_0(t)=0. \quad (55)$$

Its solutions are

$$E_n(t) = H_n(\omega_p t) e^{-\frac{(\omega_p t)^2}{2}} \tag{56}$$

with H being the Hermite polynomial, where

$$\omega_p = \sqrt[4]{\frac{\alpha_m L_m \omega_g^2 \omega_m^2}{2\alpha_g L_g}} \quad \text{and} \quad \left(1 - \frac{\alpha_l L_l}{\alpha_g L_g}\right) = (2n+1)\frac{\omega_p^2}{\omega_g^2} \tag{57, 58}$$

In general, $\alpha_g L_g \gg \alpha_l L_l$, or the gain barely exceeds the loss. We then may write:

$$\left(\frac{\alpha_g L_g}{\alpha_l L_l} - 1\right) = (2n+1)\frac{\omega_p^2}{\omega_g^2}\frac{\alpha_g L_g}{\alpha_l L_l} \approx (2n+1)\frac{\omega_p^2}{\omega_g^2} \tag{59}$$

We therefore have a steady state mode-locked pulse.

The pulse width is inversely proportional to $(a_m L_m)^{1/4}$ and $w_g^{1/2}$. Here, $a_m L_m$ is the amplitude of the modulation and w_g is the gain bandwidth. The FWHM of the pulse is:

$$\text{FWHM} = \frac{2\sqrt{\ln 2}}{\omega_p}. \tag{60}$$

4.3. Passive Mode Locking

In the above-described active mode locking, an independent frequency generator is used to control the time dependent attenuation. It is difficult to match this control with the timing of the pulse. If this timing is not perfectly tuned, the δT_R will not be zero and mode lock will be lost. The solution to this problem is to make the control of the attenuation fundamentally dependent on the timing of the pulse through some nonlinear process. This is called passive mode locking, which can be done in a

number of ways. Kerr lens mode locking was the type used in this research. The effect needed is one that attenuates all the modes that are not in phase with the pulse and leaves the pulse alone. The pulse has a much higher intensity because of the constructive interference of modes. The Kerr lens effect can be used in conjunction with a slit to satisfy the above criteria.

In some nonlinear materials, the index of refraction is dependent on the intensity of the light passing through it. In these materials, the index can be represented as $n=n_0+n_1I$. Most laser beams have a Gaussian intensity profile. An intense laser beam passing through the appropriate nonlinear material will encounter a larger index at the center of the beam. This forms an intensity dependent lens known as a Kerr lens. If we place this Kerr lens in front of a slit of the appropriate size as depicted in fig n, the low intensity light will be attenuated by the slit. But, when the pulse passes through, the beam focuses and passes through the slit unaffected [17]. The two situations described above are depicted in Figure 11 below.

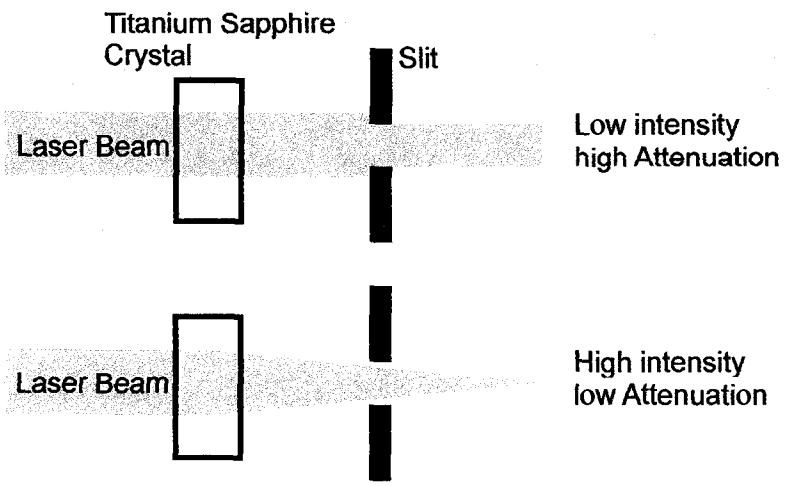

Figure 11. Kerr lens beam attenuator.

This matches the pulse and attenuator timing. In the derivation above, this is equivalent to holding δT_R at zero.

4.4. Dispersion Compensation

When different wavelengths travel at different speeds in a medium, an effect called dispersion is present. In most materials, shorter wavelengths propagate slower than longer wavelengths. This is known as positive group velocity dispersion. Most materials that the beam travels through in the cavity introduce positive group velocity dispersion. As a result, the pulse becomes chirped. The objective of the laser cavity is to generate short mode-locked pulses. Chirping will destroy this. So, we must compensate for the dispersion using a medium with negative group velocity dispersion. We could use other materials with negative group velocity but, for practical reasons, it is simpler to use the below-described prism setup.

Prisms have the useful property of bending light depending on its wavelength. Short wavelengths are bent less than longer ones. We can setup a configuration of prisms as shown below to generate a negative group velocity dispersion medium. The shorter wavelength has a shorter path to travel so, after it exits, it is now ahead of the longer wavelengths.

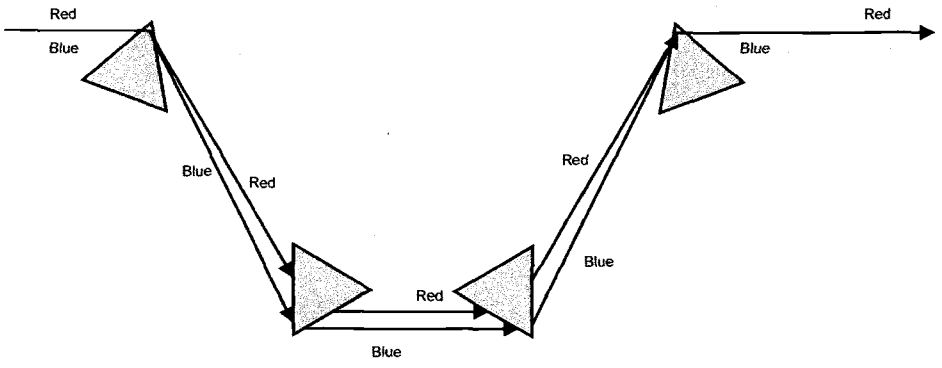

Figure 12. Four-prism dispersion compensator.

Figure 12 illustrates how negative group velocity dispersion can be achieved using prisms. But, in practice and in the laser used in this experiment, the same results can be achieved by using just two prisms and a mirror. The mirror causes the light to

travel back through the first two prisms. This serves the purpose of the second set of prisms, which is to recombine the beams, as illustrated below in Figure 13.

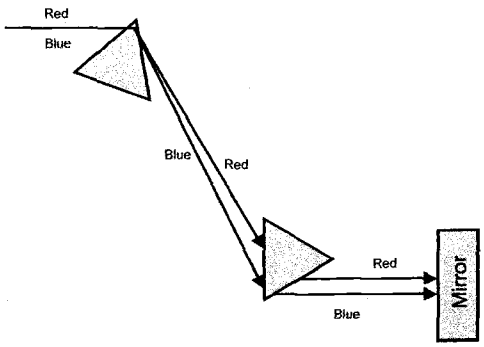

Figure 13. Two-prism dispersion compensator.

5. EXPERIMENT

5.1. Experiment Setup

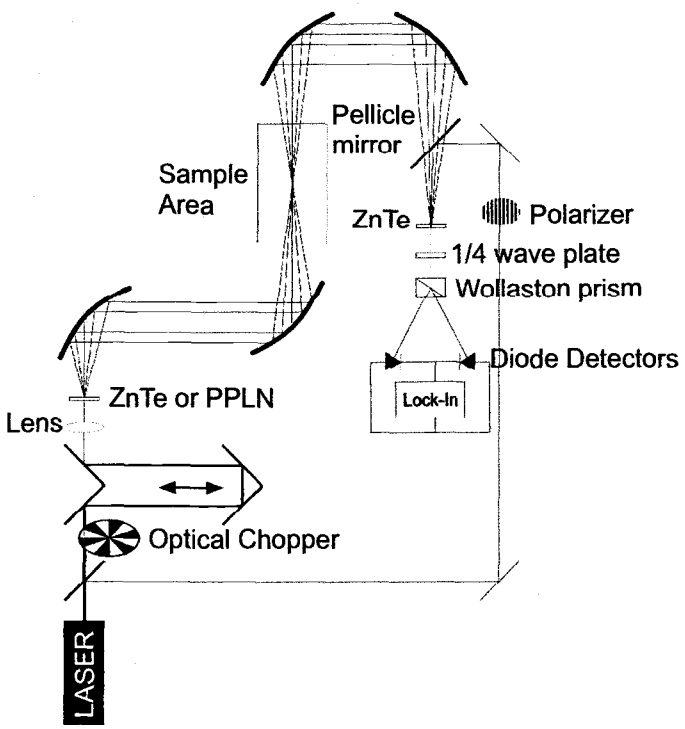

Figure 14. THz experimental setup

The diagram in Figure 14 is of the experimental setup utilized in our pulse shaping experiments. Starting from the laser, the beam is split into two paths: a pump and a probe. The pump, which is the bulk of the energy, is responsible for the THz generation. This path first passes through an optical chopper to modulate the beam for the lock-in amplifier. Then it passes through a linear track to vary the path length before it passes through the ZnTe crystal. The THz radiation is divergent, so we use off-axis parabolic mirrors to guide the THz. At the end of path, the THz is recombined with the probe beam through a pelago beam splitter. Together, the THz and optical probe beam travel through the ZnTe. The THz field has the effect of rotating the polarization of the probe beam as described in the electro-optic section above. After that, the probe passes through the quarter wave plate and is split into x and y polarization in the Wollaston prism. Each polarization is measured in their respective photo diodes.

5.2. Coherent Control

For many of the envisioned applications of THz technology, the ability to generate and manipulate the radiation in a variety of formats is required. For example, temporally shaped pulse trains will be needed for communications, signal processing and quantum control, broadband pulses for remote sensing and materials characterization, and tunable narrow-band radiation for imaging. The need for such pulses in the THz regime is further motivated by their routine use in both optical and radio frequency applications.

The application of pulse shaping that most interests us is the coherent control of gases and solid materials with phase locked pulses [18]. When an ensemble of quantum states is excited coherently and allowed to evolve in time, the coherence has a finite lifetime. This lifetime is due to the fact that the states in the ensemble are not identical and will oscillate at slightly different frequencies. As a result, coherence is a transient state. To conduct experiments to interact with this coherence, the pulse duration must

be shorter than the dephasing time. The phase of optical light pulses is important in interaction with matter when the dephasing times of the optical transitions are longer than pulse duration and temporal separation of the pulses. Under these conditions, the relative phase between successive incident pulses strongly influences the dynamic evolution of the quantum system. Femtosecond lasers are fast enough to make it possible to perform these types of coherent control experiments. If we send a pulse into a material, a polarization is created in phase with the incident light. The radiation from this polarization is its second derivative with respect to time. This creates a phase shift of Pi between the incident and radiated light. If we send two pulses into the material, wherein the second phase is locked with the first, the second pulse interferes with the polarization. When the second pulse constructively adds to the polarization, we expect its absorption to be enhanced. On the other hand, when it destructively interacts with the polarization, the energy stored in the polarization will be removed from the system and added to the second pulse. This phenomenon has not been widely studied because most experiments focused on the coherent control of the excited system and not on the control of the pulses themselves.

An earlier experiment carried out at this laboratory demonstrated this type of phase control [19]. In that experiment, two broadband pulses were used so multiple transitions were excited at the same time. This is a demonstration of pulse shaping techniques that will be used to control a single transition. For this, we will need narrow band pulses. To achieve this, we will use our fanned-out PPLN sample and a Mach-Zender interferometer to split the pulse as shown in Figure 15 below.

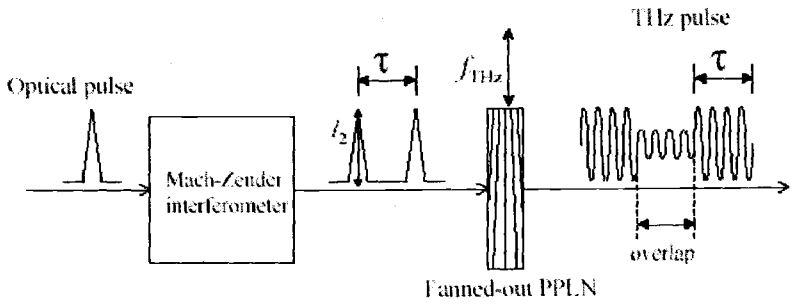

Figure 15. Pulse-shaping apparatus

This setup gives us a lot of adjustability. The frequency can be adjusted by moving the fanned-out PPLN crystal. The relative phase can be adjusted using the Mach-Zender interferometer, and the amplitude of the pulses can be adjusted by putting an attenuator in one of the paths of the interferometer.

5.3. THz Synthesis via Optical Rectification of Shaped Ultra Short Pulses

Using the techniques described above, we have conducted an experiment to demonstrate the generation and detection of narrowband THz pulses with controllable relative phase.

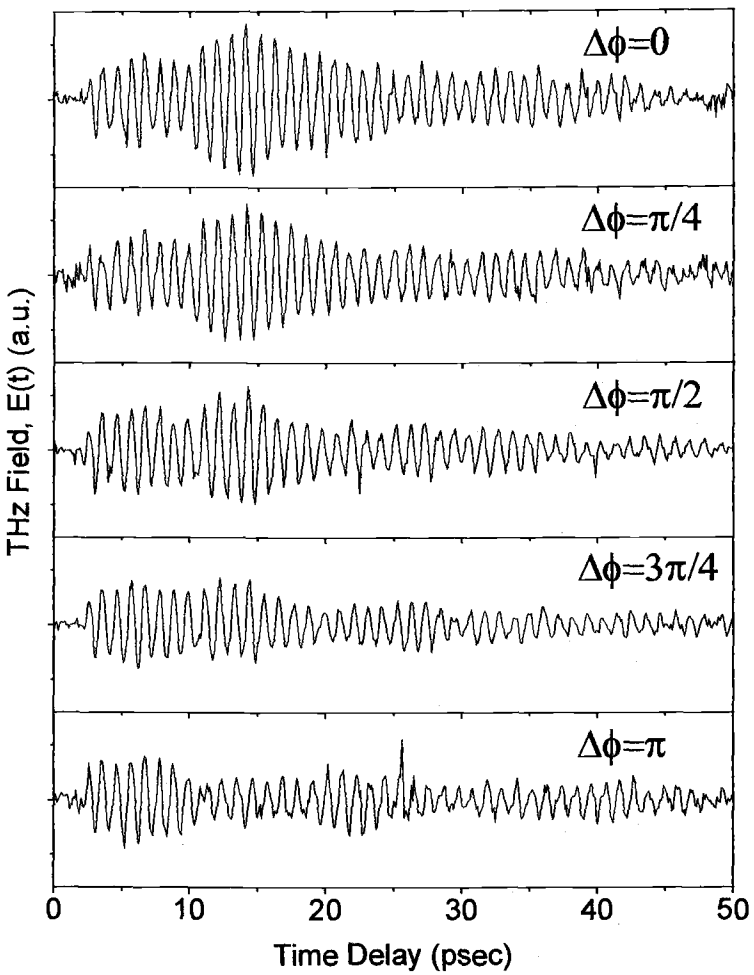

Figure 16. Terahertz pulse-shaping experimental data.

Figure 16 shows the interference of two THz pulses of varying phase shift. The THz pulses were generated using two 100 fs optical pulses with a central frequency of 820 nm. Using the interferometer, the phase has been adjusted from 0 to Pi. This phase adjustment has been made to within 2 μm. We observe constructive interference with $\Delta\Phi=0$ and destructive with $\Delta\Phi=Pi$. The above-discussed coherent control experiments will require narrowband pulses with specific relative phase and amplitude. In this experiment, we have demonstrated control over these parameters.

To further verify that we are indeed looking at interference effects of two pulses, and that the relative phase is accurate, we have simulated the THz generation in the PPLN sample. This was done by numerically solving the one-dimensional wave equation introduced in the PPLN section above. By adjusting the phase of the optical pulses, as we did in the experiment, we can verify the behavior seen in the data is that of two overlapping pulses.

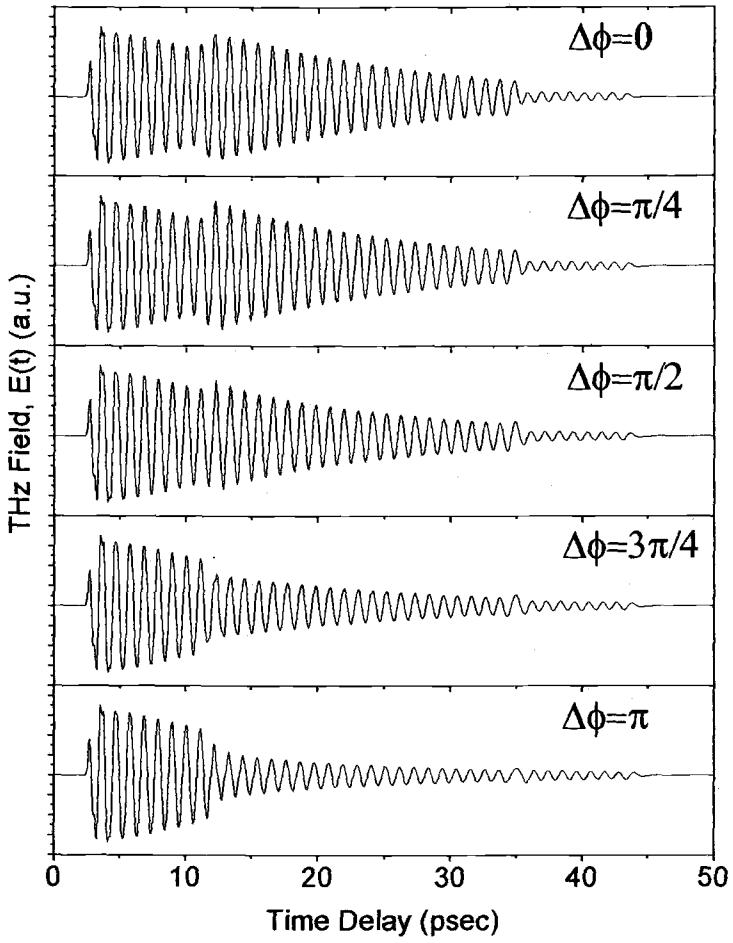

Figure 17. Terahertz pulse-shaping simulation data

As in the experimental results, the phase has been adjusted from 0 to Pi. The pulse shape observed in Figure 17 is the same as in the data verifying both the source of the pulse shaping and the relative phase.

For further verification, we can look at the Fourier transform of the wave packet. The transforms in Figure 18 below are plotted for the same range of phase shift as before.

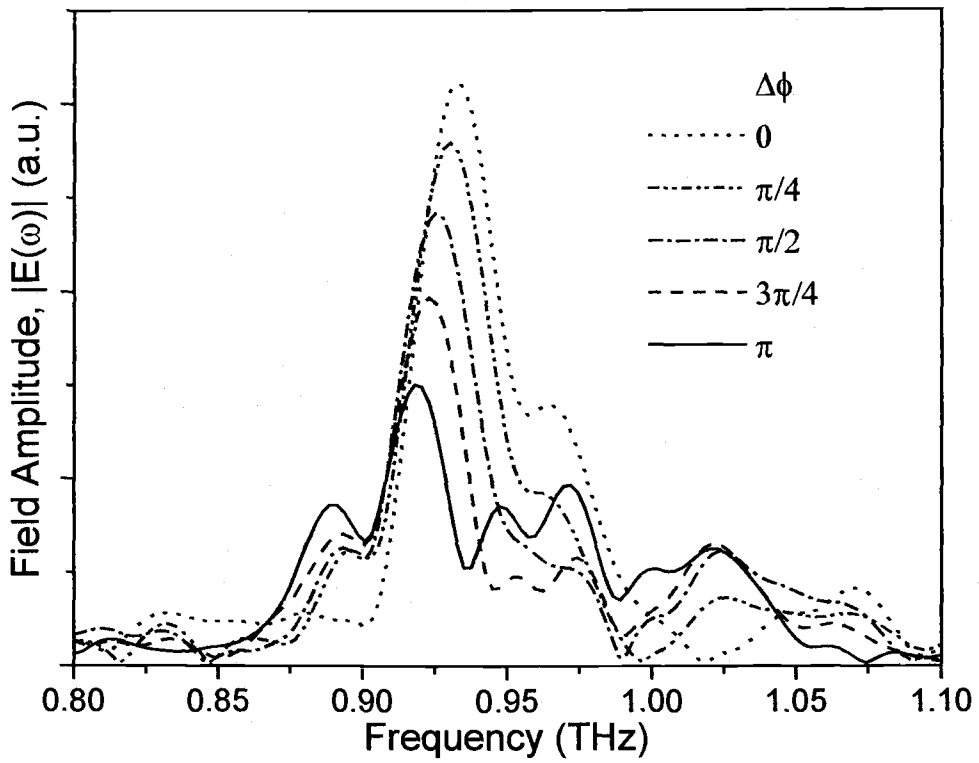

Figure 18. Fourier transform of experimental terahertz-shaped pulses.

The above plot shows the Fourier transform of the experimental data over that same range of phase shifts, from 0 to Pi. The most notable aspects of the data are (1) the consistent spectral shift from .94 THz down as the phase shift increases, and (2) the spectrum broadens as the interference becomes more destructive. The same transform has been made to the simulation data for comparison.

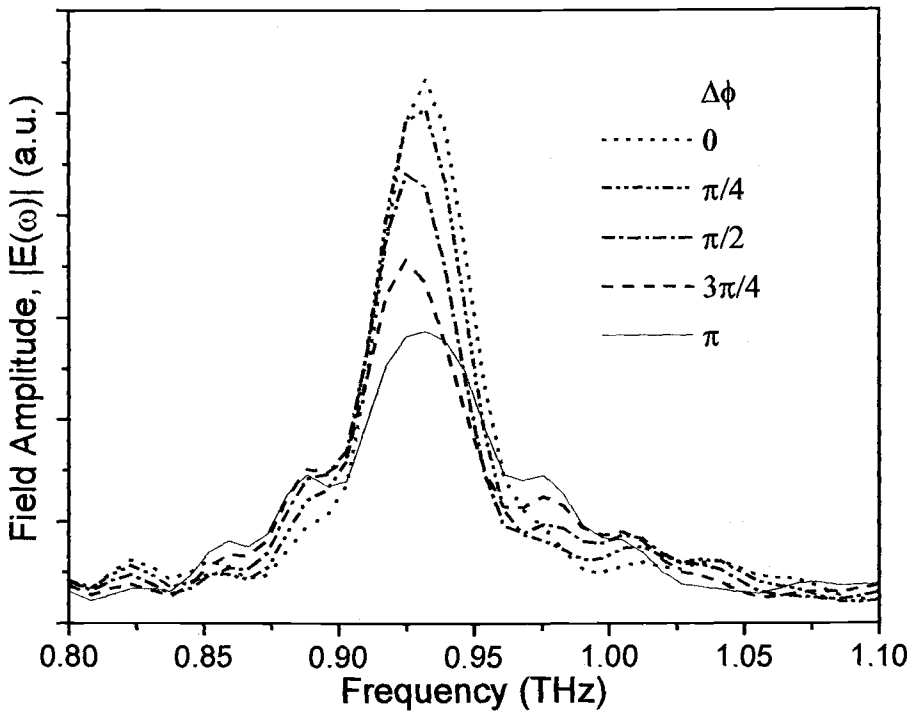

Figure 19. Fourier transform of simulated terahertz-shaped pulses.

In Figure 19, transforms of the simulation data, the same trends can be seen. As we move off zero phase shift, the spectrum shifts down and broadens.

6. CONCLUSION

Coherent control of molecular rotational transitions using shaped THz pulses has been demonstrated [19]. In this experiment, multiple transitions were excited simultaneously. Our long-term objective is to have the ability to control one transition at a time. To achieve this, multi-cycle narrowband pulses must be used. Also, adequate control of the pulses' relative phase and amplitude must be achieved. In this experiment, we have generated such pulses and demonstrated sufficient control of the phase.

REFERENCES

[1] W. H. Knox, R. L. Fork, M. C. Downer, R. H. Stolen, and C.V. Shank, "Optical Pulse Compression to 8 fs at a 5-kHz Repetition Rate," Appl. Phys. Lett. 46, 1120-1121 (1985).

[2] R. W. Boyd, *Nonlinear Optics*, 2nd Ed. (Academic Press, San Diego, 2003), pp. 87-93.

[3] C. W. Luo, K. Reimann, M. Woerner, T. Elsaesser, R. Hey, and K. H. Ploog, "Rabi Oscillations of Intersubband Transitions in GaAs/AlGaAs MQWs," Semicond. Sci. Technol. 19, S285–286 (2004).

[4] M. Walther, P. Plochocka, B. Fischer, H. Helm, and P. U. Jepsen, "Collective Vibrational Modes in Biological Molecules Investigated by THz Time-Domain Spectroscopy," Biopolymers (Biospectroscopy), 67 (4-5), 310-313 (2002).

[5] L.Thamizhmani, A.K.Azad, Jianming Dai and W.Zhang, "Far-Infrared Optical and Dielectric Response of ZnS Measured By Terahertz Time-Domain Spectroscopy," Appl. Phys. Lett. 86, 131111-1-3 (2005).

[6] THz T. Hattori, K. Ohta, R. Rungsawang, and K. Tukamoto, "Phase-Sensitive High-Speed THz Imaging," J. Phys. D: Appl. Phys. 37(5), 770-773 (2004).

[7] H. Nemec, A. Pashkin, P. Kuzel, M. Khazan, S. Schnüll, and I. Wilke , "Carrier Dynamics in Low-Temperature Grown Gaas Studied by THz Emission Spectroscopy," Journal of Applied Physics 90, 1303 (2001).

[8] T.-I. Jeon, K.-J. Kim, C. Kang, S.-J. Oh, J.-H. Son, K.-H. An, D. J. Bae, and Y. H. Lee, "Terahertz Conductivity of Anisotropic Single Walled Carbon Nanotube Films," Appl. Phys. Lett. 80(18), 3403-3405 (2002).

[9] Z. Jiang, M. Li, and X.-C. Zhang, "Dielectric Constant Measurement of Thin Films by Differential Time-Domain Spectroscopy," Appl. Phys. Lett. 76, 3221-3223 (2000).

[10] D. H. Auston, K. P. Cheung, J. A. Valdmanis, and D. A. Kleinman, "Cherenkov Radiation from Femtosecond Optical Pulses in Electro-Optic Media," Phys. Rev. Lett. 53, 1555-1558 (1984).

[11] H. A. Haus, *Waves and Fields in Optoelectronics*, (Prentice-Hall, New Jersey, 1984), pp. 339-346.

[12] Y.-S. Lee, T. Meade, V. Perlin, H. Winful, T. B. Norris, and A. Galvanauskas, "Generation of Narrowband Terahertz Radiation via Optical Rectification of Femptosecond Pulses in Periodically Poled Lithium Niobate," Appl. Phys. Lett. 76, 2505-2507 (2000).

[13] Y.-S. Lee, N. Amer, and W. C. Hurlbut, "Terahertz Pulse Shaping via Optical Rectification in Poled Lithium Niobate," Appl. Phys. Lett. 82, 170-172 (2003).

[14] D. Mittleman, *Sensing with Terahertz Radiation*, (Springer, Berlin, 2003), pp. 161-162.

[15] E. Hecht, *Optics*, 3rd Ed. (Addison Wesley Longman, New York, 1998), p. 139.

[16] W. T. Silfvast, *Laser Fundamentals*,(Cambridge University Press, New York, 1996), pp. 368-373.

[17] Coherent Laser Group, *Operator's Manual The Coherent Mira Model 900-F Laser*, (1997), pp. 7.1-7.17.

[18] H. Harde, S. Keiding, and D. Grischkowsky, "THz Commensurate Echoes: Periodic Rephasing of Molecular Transitions in Free-Induction Decay," Physical Review Letters 66(14), 1834-1837 (1991).

[19] W. C. Hurlbut, N. Amer, Y.-S. Lee, J. Forstner, A. Knorr, S. W. Koch, and J. W. Nibler, "Coherent Control of THz Coherent Transients of Molecular Rotational Transitions via Shaped THz Pulses," Oregon State University, Solid State Seminar (April 28, 2004).

[20] W. C. Hurlbut, B. J. Norton, N. Amer, and Y.-S. Lee, "Manipulation of Terahertz Pulses in Nonlinear Optical Crystals via Shaped Optical Pulses," pending publication (2005).

[21] G. Gallot and D. Grischkowsky, "Electro-Optic Detection of Terahertz Radiation," J. Opt. Soc. America B 16, 1204-1212 (1999).